Computers & Geosciences 133 (2019) 104306

Contents lists available at ScienceDirect

Computers and Geosciences

journal homepage: www.elsevier.com/locate/cageo

Direct Numerical Simulations of turbidity currents with Evolutive Deposit Method, considering topography updates during the simulation☆,☆☆

Luísa Vieira Lucchese [a,*], Leonardo Romero Monteiro [b], Edith Beatriz Camano Schettini [a], Jorge Hugo Silvestrini [c]

[a] Instituto de Pesquisas Hidráulicas, Universidade Federal do Rio Grande do Sul, Av. Bento Gonçalves 9500, 91501-970, Porto Alegre, RS, Brazil
[b] Universidade do Estado de Santa Catarina, Rua Paulo Malschitzki 200, 89219-710, Joinville, SC, Brazil
[c] Escola Politécnica, Pontifícia Universidade Católica do Rio Grande do Sul, Av. Ipiranga 6681, 90619-900, Porto Alegre, RS, Brazil

ARTICLE INFO

Keywords:
DNS
Turbidity current
Evolutive deposit method
Tridisperse

ABSTRACT

It is well-known that deposits of turbidity currents can significantly change bathymetry. The deposit of a current can alter sedimentation that happens afterwards, changing the deposit shape of a turbidity current. Direct Numerical Simulations of tridisperse turbidity currents are performed considering a rectangular channel and finite-release initial condition. The results are successfully compared to numerical and experimental results. We developed the Evolutive Deposit Method (EDM), that calculates the deposited volume and updates the topography based on the accumulated deposit for a given period of time. Entrainment is not considered. EDM has an original mathematical formulation. Topography update occurs at every τ and is based on two surfaces: Ψ and Γ. Ψ is a reference surface that can only assume integer mesh nodes, and defines the location of the solid represented by Immersed Boundary Method. Γ is a signed surface in which the deposit is integrated, and that is also fed by the rounding errors of Ψ. It is observed that the error caused by not considering the changes on topography due to deposit increases with time. For the case with initial flat terrain, the turbidity current front is the same whether considering the update or not. We also performed two simulations of turbidity currents propagating over the deposits produced by a previous current. In one case, the bathymetry was updated during both the first and the second events, and, in another, only changes on bathymetry between the simulations were considered. Results show that the order of magnitude of the relative deposit error of not considering bathymetry update remains the same order for both the first and the second consecutive events.

1. Introduction

Hyperpycnal gravity currents consist of a wedge of heavy fluid intruding into an expanse of lighter fluid by the action of gravitational force (Benjamin, 1968). If the flow is driven by a density difference caused by the presence of suspended particles, the phenomenon is called a turbidity current (Simpson, 1999). Even though there are sediments in its composition, the dynamics of low-concentrated turbidity currents are mainly dictated by turbulence rather than grain interaction (Shanmugam, 2000; Parsons et al., 2007; Manica, 2009; Meiburg and Kneller, 2010).

Turbidity currents deposits, called turbidites, are of common interest for many research fields, such as stratigraphy, petroleum engineering, and fluid mechanics simulation (Meiburg and Kneller, 2010). Such turbidites are consolidated deposits from many flows, generating a complex underwater set, which involves submarine fans and channels. Specific models for different concentration and grain-size ranges were proposed to predict the gradation and the layers of these deposits (Bouma, 1962; Stow and Shanmugam, 1980; Lowe, 1982). Harris et al. (2002) developed a theoretical model for deposit and front evolution of turbidity currents that obviates the need for numerical integration, and achieved results comparable to the numerical solution of shallow-water equations. Normal to massive gradation is usually observed in an event deposit (Kuenen and Migliorini, 1950). Normal gradation is when the larger grain sizes are deposited below the smaller ones, and massive gradation is a particle grain size mix in the deposit. It is possible to predict the deposition patterns on turbidites by simulating

Abbreviations: EDM, Evolutive Deposit Method

☆ The open-source code used is Incompact3d, available at www.incompact3d.com.

☆☆ Declarations of interest: none.

* Corresponding author.
E-mail addresses: luisa.lucchese@ufrgs.br (L.V. Lucchese), leonardo.monteiro@udesc.br (L.R. Monteiro), bcamano@iph.ufrgs.br (E.B.C. Schettini), jorgehs@pucrs.br (J.H. Silvestrini).

https://doi.org/10.1016/j.cageo.2019.104306
Received 3 October 2018; Received in revised form 14 May 2019; Accepted 31 July 2019
Available online 8 August 2019

numerically the flow that generated them, and recomposing its deposit. Using numerical simulations with a polidisperse approach, it is possible to understand the deposition process and the formation of turbidites in a temporal scale.

There are several methods for turbulence representation on numerical simulations. Using a Direct Numerical Simulation (DNS) means turbulence models are not employed, because they are not needed when mesh sizes chosen are small enough to capture the highest wavenumbers (smallest eddies) of turbulence energy cascade (Lesieur, 2008). Therefore, DNS provides an accurate turbulence simulation, because the energy dissipation of the smallest scales occurs by the same mechanism as for the large eddies. Unlike other common methods such as Reynolds-Averaged Navier–Stokes (RANS) and Large Eddy Simulation (LES), DNS brings the possibility to simulate all turbulent scales present in a fluid flow. Turbidity currents are turbulent by definition — the sediments are sustained by turbulence rather than by other supporting mechanisms such as grain interaction (Shanmugam, 2000). Therefore, turbidity currents are possible subjects of study and would benefit from DNS. Another characteristic of DNS is its spatial discretization. Because mesh sizes tend to be much smaller in DNS than in methods that use modeled turbulence (such as RANS and LES) (Lesieur et al., 2005), the resolution of the deposit tends to be better. Also, the turbulent flow of the turbidity current is solved directly in all turbulent scales, bringing possibly more accurate results.

Even if turbidity currents deposits have been widely studied numerically (Necker et al., 2002; Cantero et al., 2008; Nasr-Azadani et al., 2013; Guerra et al., 2013; Nasr-Azadani and Meiburg, 2014; Espath et al., 2015; Kováříik et al., 2015; Francisco et al., 2018), there are no records of DNS of turbidity currents that consider the previous time steps deposited matter in the simulation, and also no records of topography updating on two successive events. Hoffmann et al. (2015) simulated 2D turbidity currents that propagated and deposited over complex topographies, and the bottom topography is updated at the end of every simulation. Recently, Kyrousi et al. (2018) updated the topography of a turbidity current based on its deposit, but the effect of the update itself was not analyzed. Kyrousi et al. (2018) research employed Large Eddy Simulations (LES), that, unlike DNS, applies a turbulence model to the smallest turbulent scales, simulating only the largest turbulent scales present in the turbulent fluid flow. Most numerical simulations of turbidity currents do not consider the evolution of bathymetry, thus it is important to quantify the error that they can be committing when not considering topography updates. No studies on this matter were found. In this paper, we present numerical results of DNS in which the topography is updated at a given frequence of time, feedbacking the simulated domain with the so-far calculated deposit, quantifying the differences in the resulting deposit. We call this development Evolutive Deposit Method (EDM). Deposits of a simulation that employs this method are compared to one that does not. These differences are quantified and presented for four instants of time. We also simulated the propagation of a turbidity current event over the deposit of a previous one, as it happens in nature. Within this concept, we compared EDM to the approach in which the terrain is updated at the end of each simulation.

2. Methodology

The simulations are performed in a channel configuration, with finite-release initial condition (Fig. 1). The domain is rectangular (L_x, L_y, L_z) and, initially, the bottom is a horizontal layer of height h_p, over which the sediments suspended on the gravity current flows are able to accumulate. The denser fluid, in the initial condition, has a volume (X_f, h, L_z). To represent the suspended sediments, we employ dimensionless density Φ, composed by fractions of different grain-size categories simulated ($\Phi = \sum_{d=1}^{n_\Phi} \Phi_d$), defined as:

$$\Phi_d = \frac{\tilde{\rho}_d - \tilde{\rho}_{min}}{\tilde{\rho}_{max} - \tilde{\rho}_{min}}, \tag{1}$$

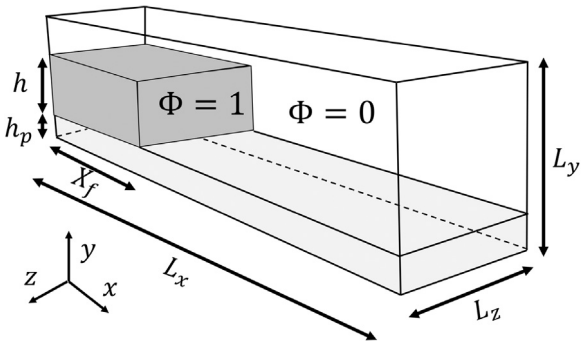

Fig. 1. Initial condition and dimensions of the simulated domain.

where $\tilde{\rho}_d$ is the density of the mix of fluid with sediments of granulometric fraction d, $\tilde{\rho}_{max}$ is the maximum density and $\tilde{\rho}_{min}$ is the minimum density at the initial condition. Dimensional quantities are denoted by a tilde. For simulation purposes we define $\Phi = 1$ for the denser fluid on the initial condition and $\Phi = 0$ for the lighter one.

Boussinesq approximation can be considered a good approximation because the cases here presented are low-concentration turbidity currents (Bagnold, 1954). The differential equations to solve the flow are non-dimensionalized with the dimensional magnitudes $\tilde{h}$, $\tilde{\rho}_{max}$, $\tilde{\rho}_{min}$, and $\tilde{u}_b$. The buoyancy velocity is $\tilde{u}_b = \sqrt{g'\tilde{h}}$, where $\tilde{h}$ is the dimensional height of the denser fluid in the initial condition, and the modified gravity $g' = \tilde{g}C_r(\tilde{\rho}_p - \tilde{\rho}_{min})/\tilde{\rho}_{min}$, being $\tilde{\rho}_p$ the grain density of the particles, $\tilde{\rho}_{min}$ the ambient fluid density, C_r the dimensionless volumetric sediment fraction of the current (Gladstone et al., 1998), and $\tilde{g}$ the local gravity acceleration. The adimensional groups obtained by non-dimensionalization procedures are Reynolds Number $Re = \tilde{u}_b\tilde{h}/\nu$ and the Schmidt number $Sc = \nu/\kappa$, where κ is the molecular diffusion coefficient and ν the kinematic viscosity. Assuming the same diffusivity and kinematic viscosity for all fluids, the Sc number becomes 1. The value of Sc was also based on the paper from Nasr-Azadani et al. (2013), that also simulated the same case from Gladstone et al. (1998). Härtel et al. (2000b) showed that Schmidt numbers equal to unity or greater than one do not affect the dynamics of the flow significantly.

Continuity, Navier–Stokes, and Scalar Transport equations in dimensionless form are:

$$\nabla \cdot \vec{u} = 0, \tag{2}$$

$$\frac{\partial \vec{u}}{\partial t} + (\vec{u} \cdot \nabla)\vec{u} = -\nabla \Pi + \sum_{d=1}^{n_\phi} \Phi_d \vec{e}_g + \frac{1}{Re}\nabla^2 \vec{u} + \vec{f} \tag{3}$$

$$\frac{\partial \Phi_d}{\partial t} + (\vec{u} + u_{s,d}\vec{e}_g) \cdot \nabla \Phi_d = \frac{1}{ReSc}\nabla^2 \Phi_d, \; d = 1, 2, \ldots, n_\phi \tag{4}$$

where $\vec{u}$ is the velocity field, t is time, $\vec{e}_g = (0, -1, 0)$ is a versor in the gravity direction, Π is the normalized pressure field, and $u_{s,d}$ is the dimensionless settling velocity for each granulometric fraction d, calculated by $u_{s,d} = \tilde{u}_{s,d}/\tilde{u}_b$, for which $\tilde{u}_{s,d}$ is the dimensional settling velocity for a given particle diameter, expressed by the Stokes law (Rubey, 1933). $\vec{f}$ is a forcing term that represents the force reaction of the solid body (in this case, the terrain elevation) on the surrounding fluid.

The boundary conditions for velocity are free-slip conditions in every face, except over the bottom topography, where $\vec{f}$ forcing term ensures the no-slip condition via Immersed Boundary Method (IBM) (Peskin, 2002). An advantage of IBM is that the mesh does not need to be dynamic in order to insert a moving object (in case, the topography) inside the simulated domain. For Φ, on the boundaries of the domain

no-flux condition ($\frac{\partial \Phi}{\partial x_i} = 0$) is applied in every direction except over the bottom topography, where an internal condition is imposed via IBM. The sedimentation condition is applied as $\vec{u} = \vec{0}$ on the surface of the object, so the advection term in Eq. (4) is only influenced by the settling velocity.

The Eqs. (2), (3), and (4) are solved using *Incompact3d* code (Laizet and Lamballais, 2009; Laizet and Li, 2011). The domain is discretized in a 3D Cartesian mesh, with sixth-order finite-difference implicit compact schemes (Lele, 1992) for spatial derivatives, and third order Adams–Bashforth scheme for temporal integration. We also use 2D Message Passing Interface (MPI) for parallel processing.

The mass of sediments deposited over the bottom, after a time t, is given by:

$$D(x,z,t) = \int_0^t \sum_{d=1}^{n_\Phi} u_{s,\mathrm{d}}\ \Phi_\mathrm{d}(x,z,\tau)\ d\tau \tag{5}$$

In order to convert D into a volume of deposit, used for topography modification, a compactation factor $\sigma = C_r/(1-p)$ is applied (Nasr-Azadani et al., 2013), where p is the porosity of the turbidite. Once deposited, the sediments cannot be re-suspended by the flow. Mostly, the presented simulations are for small Reynolds numbers, that tend to present less entrainment (Necker et al., 2002).

To calculate the deposit updates, the mass deposit is integrated at each time step, and accumulated in a deposit surface $\Gamma = \Gamma(x,z,t)$, representing a surface where the deposit of each time step is accumulated. Physically, it could be observed as a value, positive or negative, representing the signed distance of the continuous deposit surface location from the discretized surface represented in the simulation, called Ψ. The surface $\Psi = \Psi(x,z,t)$ is a reference surface that represents integer mesh values in y direction, in order to define the mesh location of the bottom surface for simulation purposes. This reference surface must be located over the mesh nodes, so it can only assume integer mesh values. If a parallel was to be traced with Exner equation (Paola and Voller, 2005) for topography alteration, the interface between solid and fluid would be analogous to Ψ, with the difference that Ψ can only assume integer mesh values. Every interval of time τ, the bathymetry is updated, and the surface Ψ can be updated, depending on the volume sedimentated in τ. If Ψ changes, then Γ should be adjusted accordingly to compensate the rounding errors of Ψ. If $\frac{\Delta y}{2} \leq \Gamma_t + (D_{t+\tau} - D_t)\sigma < \Delta y$, Ψ surface is updated to the upper point even if the mesh cell is not completely filled with sediments, and $\Gamma_{t+\tau}$ assumes a negative value to be compensated in the next update (Fig. 2a). If the mesh cell is overfilled by deposit, Ψ is updated to the upper point and Γ receives the value of the deposit excess in relation to Ψ (Fig. 2b). When Ψ is updated to the upper point, all sediments located within the transition area are accounted as deposit. On Fig. 2 one can see an illustration of the developed method. The general scheme for EDM is:

$$\Gamma_{t+\tau} = \begin{cases} \Gamma_t + (D_{t+\tau} - D_t)\sigma, & if\ \ \Gamma_t + (D_{t+\tau} - D_t)\sigma < \dfrac{\Delta y}{2}, \\ \Gamma_t + (D_{t+\tau} - D_t)\sigma - \Delta y, & if\ \ \Gamma_t + (D_{t+\tau} - D_t)\sigma \geq \dfrac{\Delta y}{2}. \end{cases} \tag{6}$$

The value $\Gamma_t + (D_{t+\tau} - D_t)\sigma$ must be smaller than $\frac{3}{2}\Delta y$ so that the reference surface Ψ does not jump two meshes at a time, avoiding important changes on the velocity field, and so time intervals τ must be adjusted accordingly to assure that. τ is usually set to a much lower value than the average time necessary to fill one mesh vertically. The topography can be, as well, updated at each time step, but this would be, for most cases, a waste of computational resources because the update on IBM is a costly operation.

DNS are performed for all simulations but the one that resembles Gladstone et al. (1998) experiment, because the original Re for this case was too high. In this simulation, sub-eddy hyperviscosity was modeled using the method of Dairay et al. (2017).

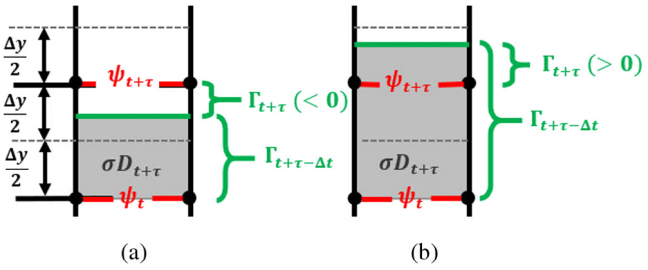

Fig. 2. Deposit evolution and topography update scheme, for each (x,z) coordinate. Deposited volume Γ changes when Ψ is updated, and can either become (a) negative, representing a deposit deficit relative to the reference surface Ψ, or (b) positive, representing an excess of deposit relative to Ψ. τ is the interval between two successive bathymetry updates.

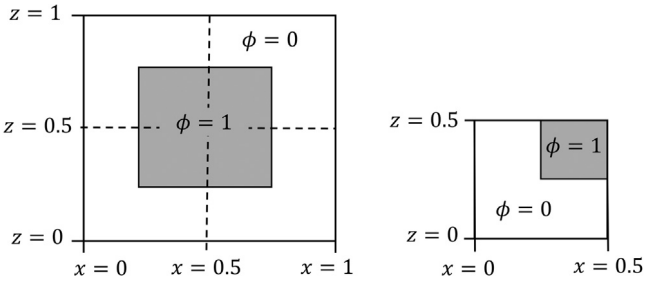

Fig. 3. Schema of the verification domain and one quarter of it.

3. Validation and verification

Even if *Incompact3d* code is already validated for gravity currents (Espath et al., 2014, 2015; Francisco et al., 2017), some new verifications and validations are needed, because the new method changes the bathymetry. A verification of the lateral free-slip boundary conditions is proposed to quantify the numerical error in deposits, caused by boundary conditions. Validations with the results of Gladstone et al. (1998) and Nasr-Azadani and Meiburg (2014) are also performed.

The boundary conditions for x and z directions are verified using a domain with double symmetry and comparing its deposit with the deposit of one quarter of it (Fig. 3). The complete domain has $L_x = 1$, $L_y = 1.1$ ($h_p = 0.1$), $L_z = 1$ and the mesh is $N_x = 101$, $N_y = 101$, $N_z = 101$. One quarter of the domain has $L_x = 0.5$, $L_y = 1.1$ ($h_p = 0.1$), $L_z = 0.5$, and spatial mesh size is the same. In the initial condition, a cubic volume of dense fluid ($\Phi = 1$), measuring $(0.5, 1, 0.5)$ is initially positioned in the center of the domain. In one quarter of the domain, it is positioned in the corner to keep similarity between simulations. The difference in deposit volume between these simulations remains in order of machine accuracy, which is on order of 10^{-16} for double-precision variables (Fig. 4). Thus, we can assume there is no influence of the free-slip boundary conditions in the deposit fields.

We compare our model with a numerical simulation that computed the propagation of a turbidity current over a Gaussian bump (Nasr-Azadani and Meiburg, 2014). For this comparison, we used a domain with $L_x = 20$, $L_z = 3$ and $L_y = 2.2$, where the bottom platform under the bump is 0.2 thick. The bump height is 0.25 and its center is located at $x = 5.5$. Meshes are $1025 \times 129 \times 97$, and $Re = 2000$. The simulation is discretized in two particle diameter sizes, it is therefore called a bidiperse simulation, with $u_{s,1} = 0.03$ and $u_{s,2} = 0.006$. The accounted quantity for deposit is the sedimentation rate $D^*_\mathrm{d}(t)$, shown below:

$$D^*_\mathrm{d}(t) = \int_0^{L_z} \int_0^{L_x} u_{s,\mathrm{d}}\ \Phi_\mathrm{d}(x,z,t)\ dx\ dz. \tag{7}$$

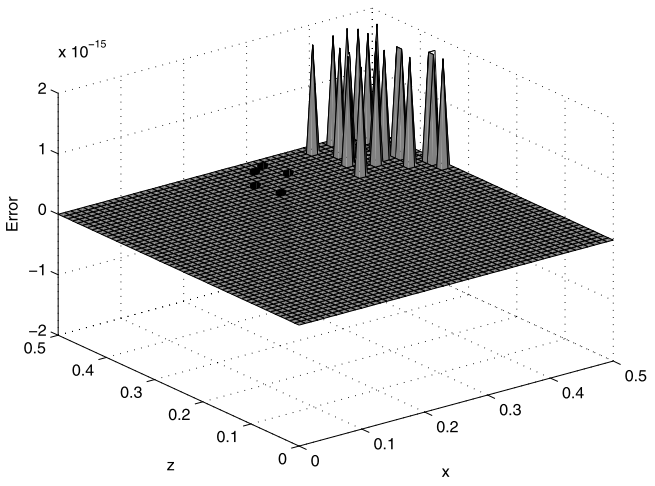

Fig. 4. Difference between the deposits of the test domain used in the verification and one quarter of it.

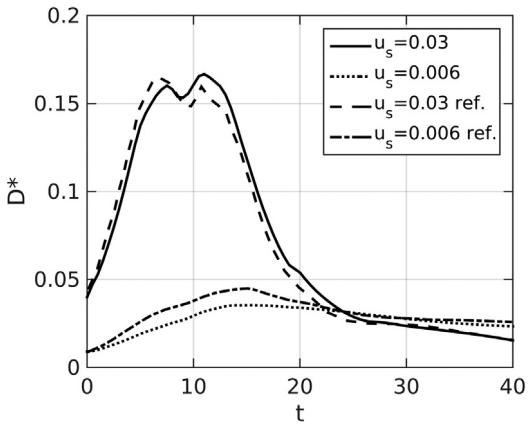

Fig. 5. Sedimentation rate along time. Comparison between Nasr-Azadani and Meiburg (2014) and the present results.

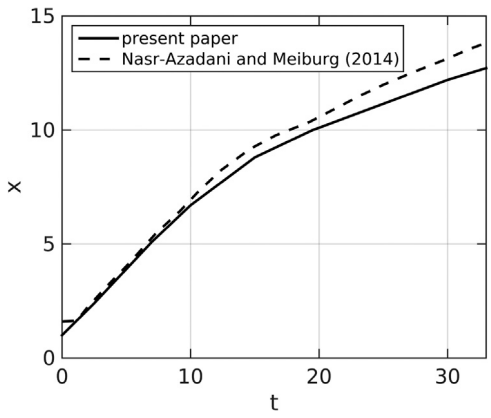

Fig. 6. Front position along time. Comparison between Nasr-Azadani and Meiburg (2014) and the present paper.

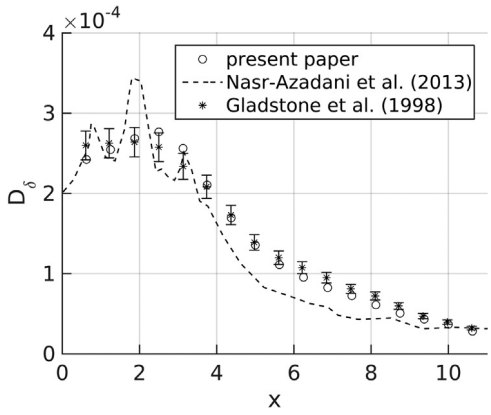

Fig. 7. Comparison between the deposit density (D_δ) of Gladstone et al. (1998) experiments, Nasr-Azadani et al. (2013), and the present study. Typical uncertainties for the experimental results are plotted as errorboxes.

The comparison with Nasr-Azadani and Meiburg (2014) is shown in Fig. 5. The results for D^* are similar to those of Nasr-Azadani and Meiburg (2014), with a small difference at the peak position. After $t = 25$, the results are very close. The maximum difference is of 6% for $u_s = 0.03$ and 26% for $u_s = 0.006$.

The temporal evolution of front position is also compared in Fig. 6. The turbidity current position of the present simulation shows satisfactory agreement with results from Nasr-Azadani and Meiburg (2014).

We also performed comparisons with the accumulated deposit of experimental (Gladstone et al., 1998) and numerical results (Nasr-Azadani et al., 2013). Dimensional height adopted for nondimensionalization is $h = 0.4$ m, which makes the physical domain $14.25 \times 1.0 \times 0.5$. The bottom platform is $h_p = 0.1$. Reduced gravity is $\tilde{g}' = 7.6$ cm/s^2, given by Gladstone et al. (1998), resulting in $\tilde{u}_b = 0.174$ m/s. Settling velocities estimated by Gladstone et al. (1998) are divided by $\tilde{u}_b$, resulting $u_{s,1} = 0.0333$ and $u_{s,2} = 0.0043$. Each one composes 50% of the initial mass fraction, reproducing experiment D of Gladstone et al. (1998). The Reynolds number calculated for this case is $7 \cdot 10^4$, that was prohibitive, therefore, in order to reduce the computational cost, $Re = 4 \cdot 10^4$ had to be adopted. An hyperviscous operator mimic of Spectral Vanishing Viscosity (SVV) Large Eddy Simulation (LES) (Dairay et al., 2017) was adopted for this specific case to adjust the simulations to the available computational power. The employed mesh is $(N_x, N_y, N_z) = (1153, 193, 97)$. The simulation uses EDM, for which the porosity of the deposit is $p = 0.35$, and the volumetric fraction of $C_r = 3.49 \cdot 10^{-3}$, volumetric concentration of 0.349% (Boussinesq is applicable), resulting in a compacting factor of $\sigma = 0.005369$. At the end of the simulation, at $t = 55$, the maximum change on the bottom topography is $1\Delta y$. The computed quantity is called by Gladstone et al. (1998) as the deposit density (D_δ), which is an average of the deposited mass of sediment on the measured area, in case, a circular cylinder. To make sure the measurement is similar to the experimental case, circular samples of radius $r = 0.104$ of the resulting deposit are extracted and the average deposit density is calculated. These samples are taken at each 0.625 dimensionless length units, starting on the finite-volume release.

Comparisons of the deposit density acquired by the present authors and the experimental and numerical results of other authors are presented in Fig. 7. Nasr-Azadani et al. (2013) simulated numerically the same case based on Gladstone et al. (1998), even though the numerical approach was different and the simulation was bidimensional. There is a good agreement, even if there are some spots in which the difference between Gladstone et al. (1998) data and the present results are larger than the presumed errors.

In Fig. 8, we present the deposit densities for the two particle fractions separately, for the same case. For the smaller particles, there are some differences for $x < 7$. This issue can be caused by the discretization used for this case, and because bedload is not accounted, and possibly it is an important phenomenon in this case. Another possible reason is the fact that our method does not consider possible re-suspension of deposited matter. Also, variability of particle sizes in the original experiment is not considered in our simulations. The

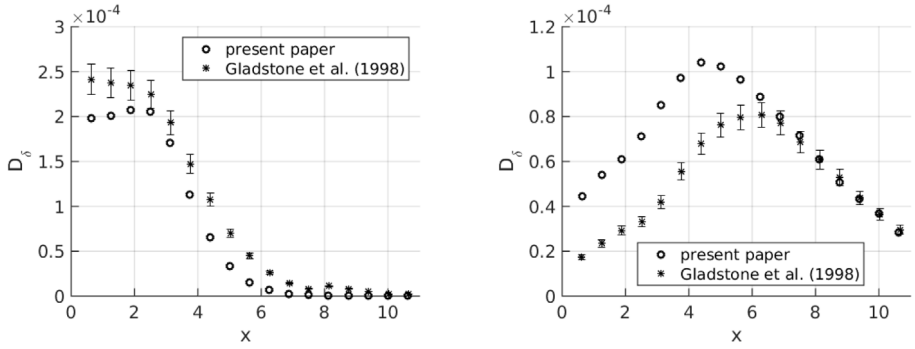

Fig. 8. Comparison between the deposit density (D_δ) of Gladstone et al. (1998) and EDM, separately for the two particle sizes. Typical uncertainties for the experimental results are plotted as errorboxes.

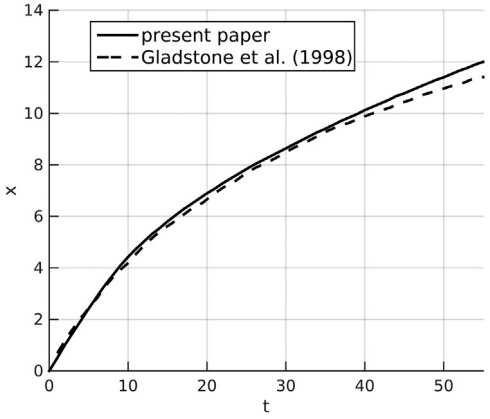

Fig. 9. Front evolution of Gladstone et al. (1998), and for the present analysis.

standard deviation of this variability for each grain size is $1.2d_{avg}$, in which d_{avg} is the average diameter.

The front position is as well compared with Gladstone et al. (1998) (Fig. 9). The fronts evolved at similar rates and velocities. Overall, validation with Gladstone et al. (1998) results is considered satisfactory.

4. Deposit of a single event

In order to analyze the differences caused by bathymetry updating in a single event, we perform simulations F1 and U1 for comparison. The simulation F1 has a flat bottom topography, modeled by an IBM platform with $h_p = 0.3$. Simulation U1 starts with the same flat terrain, but topography is updated at each $\tau = 0.01$. The domain for both simulations has $L_x = 15$, $L_y = 1.5$, and $L_z = 1.5$, and $\Delta x = 0.013$, $\Delta y = \Delta z = 0.010$, the Δt used is 10^{-4} and it is simulated until $t = 20$. The initial lock-exchange has dimensions of $2 \times 1 \times 1.5$. Both F1 and U1 are tridisperse simulations, with $u_{s,1} = 0.01$ at a initial concentration of 70%, $u_{s,2} = 0.003$ of 20% and $u_{s,3} = 0.001$ of 10%. The compactation factor used in U1 is $\sigma = 0.5$. In the analysis here presented, three grain sizes are used to simulate each current. Even if the code was verificated for bidisperse currents, the methodology is the same, no matter how many grain sizes are employed. Any (integer and positive) number would be valid.

The EDM terrain updating effects are analyzed by a comparison of cases in which the deposit is updated while the turbidity current propagates (U1 and U2), and cases in which this update is not performed (F1 and F2). In Table 1 we present a summary of the presented cases. F1 and U1 are turbidity currents that propagate over an initially flat surface, while F2 and U2 propagate over the deposits of F1 and U1, respectively. F1 and F2 events do not use EDM, while U1 and U2 do.

Table 1
Cases presented in the present study.

Simulation	Initial bathymetry	EDM
F1	Flat surface	No
U1	Flat surface	Yes
F2	Deposit of F1	No
U2	Deposit of U1	Yes

Table 2
Differences in mass deposit between U1 and F1.

Time	Mean dif.	Relative mean dif.	Max. dif.	Relative max. dif.
$t = 5$	$3.6 \cdot 10^{-5}$	0.43%	$9.4 \cdot 10^{-4}$	4.71%
$t = 10$	$3.7 \cdot 10^{-4}$	1.77%	$3.0 \cdot 10^{-3}$	5.88%
$t = 15$	$9.9 \cdot 10^{-4}$	2.64%	$5.1 \cdot 10^{-3}$	6.21%
$t = 20$	$2.0 \cdot 10^{-3}$	3.58%	$9.1 \cdot 10^{-3}$	10.75%

Final deposits after $t = 20$ are calculated, for which we can see (Fig. 10) that there are differences between the resulting deposits of U1 and F1. To analyze it in detail, absolute differences on deposit surfaces for each 5 times are computed, for both simulations F1 and U1. Fig. 10 shows the absolute differences on the accumulated deposit ($D_{U1} - D_{F1}$) between both simulations, in four moments. Average deposits on spanwise direction for times 5, 10, 15 and 20 are plotted in Fig. 11. The magnitude of the absolute differences in deposit increases with time. In $t = 5$ and $t = 10$, the higher differences occur in the propagation region, near the turbidity current front. Until $t = 10$, case U1 deposited more than F1 in all of the region where the current already propagated over, and the shape of the deposit is different. In $t = 15$, deposit differences become less concentrated on the finite release area, and the generation of deposit shape by lobe and cleft structures (Härtel et al., 2000a) is increased. In $t = 20$, it is also possible to observe lobe and cleft marks on the differences between the two deposit surfaces.

The average and maximum differences in deposit are also analyzed. In Table 2, the differences in deposit ($D_{U1} - D_{F1}$) for $t = 5$, $t = 10$, $t = 15$ and $t = 20$ are shown. The relative maximum differences are calculated as $max(\frac{D_{U1}}{D_{F1}} - 1)$. The absolute and relative differences between the deposits of U1 and F1 increase with time. The longer the duration of the event, the more important it is to implement a model that considers updates on topography during the simulation.

The effects of not considering deposit feedback are not restricted to deposit magnitude and shape. Considering the resulting fields for simulations U1 and F1 after $t = 20$, we compared local velocity fields in the three directions (Table 3), showing that the velocity fields of a current can be altered by updating the terrain.

We also compute the differences on total mass of suspended particles, at $t = 20$, between U1 and F1, taking F1 as the base data (Table 4). The suspended particles are calculated by integration of Φ_d

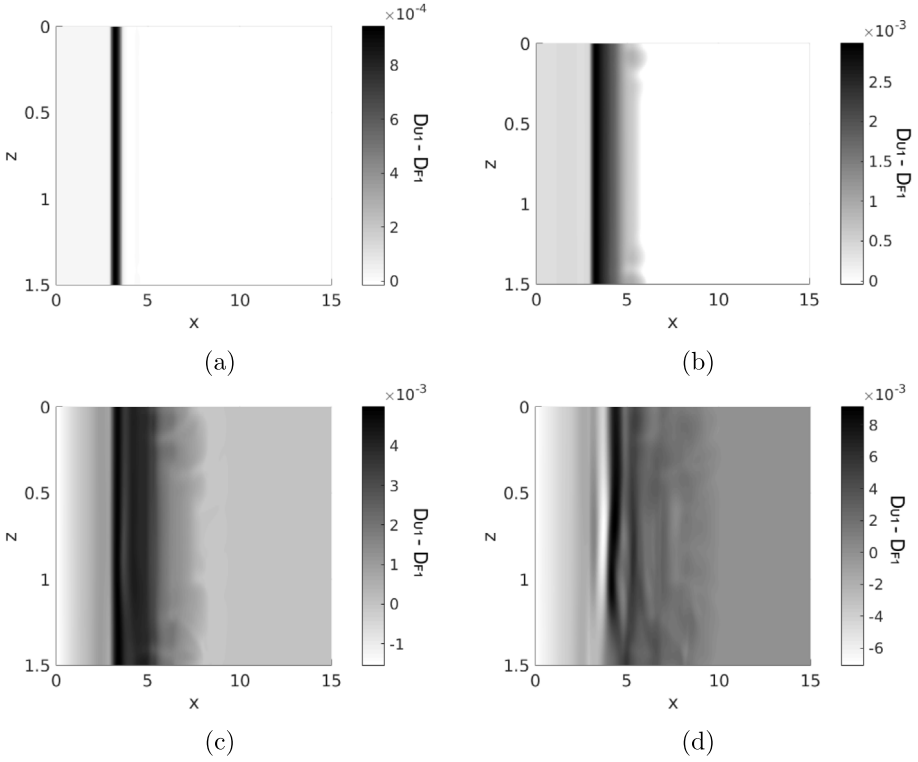

Fig. 10. Absolute differences in the deposited volume between simulations U1 and F1 ($D_{U1} - D_{F1}$), at (a) $t = 5$, (b) $t = 10$, (c) $t = 15$ and (d) $t = 20$.

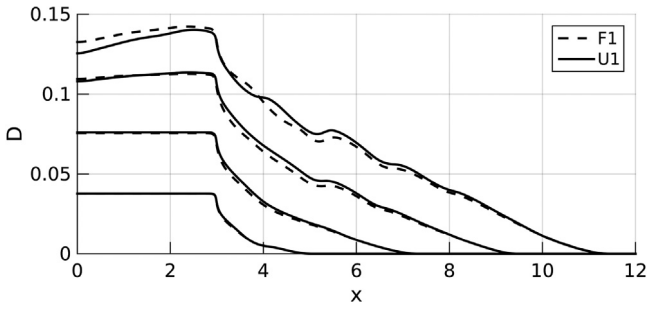

Fig. 11. Deposit curve averages on z direction, for cases F1 and U1, at $t = 5$, $t = 10$, $t = 15$ and $t = 20$ (curves from bottom to top).

Table 3
Mean differences on velocities between cases U1 and F1, at $t = 20$.

Velocity	Mean difference	Relative mean difference
u_x	0.0187	17.62%
u_y	0.0148	50.13%
u_z	0.0090	65.54%

on the domain (except over and inside the deposit). The difference is computed separately for the three granulometric fractions, though the errors are rather small and all of the same order. Case F1 has more suspended particles for the three particle diameters. This is probably due to the fact that the interface between fluid and solid tends to be higher in simulation U1, therefore the fluid flow is closer to the topography, facilitating sedimentation in U1.

In order to observe the front propagation of F1 and U1, isosurfaces of dimensionless density $\Phi = 0.4$ are plotted in Fig. 12 for times 10, 15 and 20. These isosurfaces are observed from a top view, so that one can see clearly the interface between denser and lighter fluid. To ensure the possibility of a direct comparison, the lighting applied to the six views is constant. It is observed that the turbidity currents fronts are

Table 4
Differences in total suspended mass of particles between U1 and F1, at $t = 20$.

$u_{s,d}$	dif.	Relative dif.
0.001	−0.0014	−0.30%
0.003	−0.0031	−0.34%
0.01	−0.0152	−0.56%

similar, and the lobe-and-cleft surfaces (Härtel et al., 2000a) are on the same position and configuration for simulations F1 and U1. This can have happened because both fronts propagate over a flat surface, since the bottom updates only affect regions in which the current front has already passed by. The most remarkable differences between F1 and U1 in these isosurfaces are in the body area of the current, in which some changes can be observed in the vortex pattern, specially in $t = 15$ and $t = 20$. Vortexes in the body area of the current, caused by the alteration in bottom topography, affect the interface between denser and lighter fluid. This effect can be seen in $t = 15$ (Fig. 12b), between $x = 3$ and $x = 7$, and in $t = 20$ (Fig. 12c), between $x = 4$ and $x = 8$. In $t = 10$ (Fig. 12a), the differences are more subtle, but some alterations can be seen around $x = 5$.

5. Deposit of two events

An alternative methodology is developed for simulating various turbidity current events one over another, in which a flat-bottom current would propagate, and the resulting deposit would be introduced as the starting topography for another current. We analyze the errors introduced by not considering EDM in cases with two currents with terrain updates between them.

For this analysis, U2 and U1 deposits are compared to F1 and F2. Simulation F2 has a similar configuration to F1. Its bathymetry is fixed during time, and its initial bottom topography is defined as the final deposit of F1. The maximum deposit height achieved in the initial condition of F2 is $6\Delta y$. F2 bottom remains fixed during the simulation. To perform a fair comparison with EDM, a turbidity current propagating

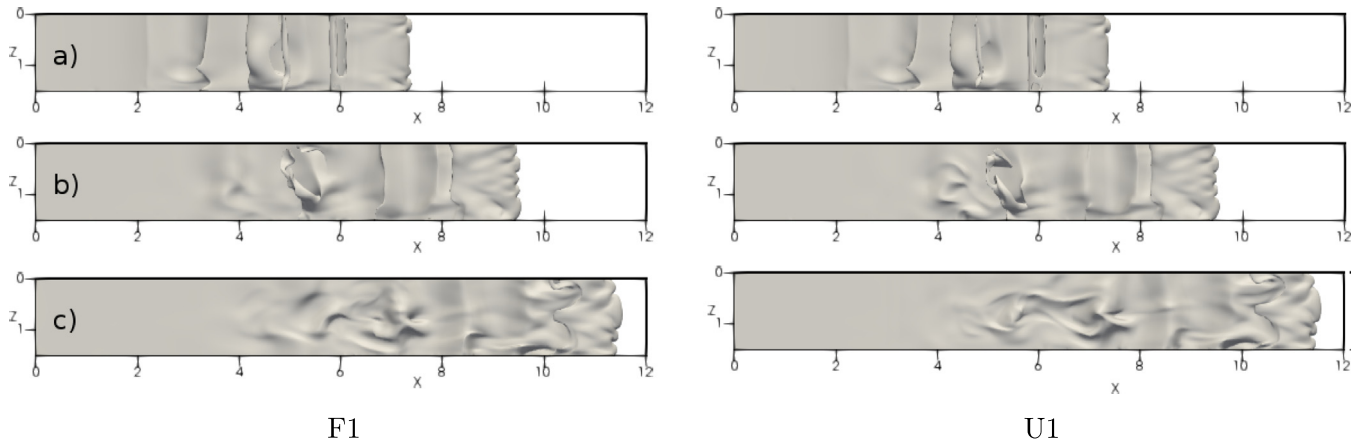

Fig. 12. Top view of isosurfaces of dimensionless density $\Phi = 0.4$, for simulations F1 and U1, at times (a) 10, (b) 15 and (c) 20. Top view.

Fig. 13. Front evolution of turbidity currents F2 (–) and U2 (–).

over the topography generated by U1 is simulated, considering EDM, with the same compactation factor as U1 ($\sigma = 0.5$), called here U2. Therefore, our goal is to compare deposits of a second event occurring over the same place as the first event, using two different approaches: F1 and F2 consider the bottom topography remains unchanged during the simulations, but is updated before the second event; U1 and U2 are the cases in which the bottom topography is updated during the simulations.

The front position along time, for simulations U2 and F2, is very similar (Fig. 13). Lobe-and-cleft structures develop differently. At $t = 20$, F2 has only two lobes, while U2 presents four. This difference is surely caused by the differences in the starting topography, which are themselves caused by differences in the final deposits of F1 and U1. Fronts of F1 and U1 are exactly the same, therefore differences in lobe-and-cleft front structures of F2 and U2 should be caused by the initial topography over which the current front propagates over.

The deposit of U2 and F2 are analyzed for times 5, 10, 15 and 20. Fig. 14 shows the average deposit on z direction for each x coordinate, generated during cases F2 and U2. The effect of not updating the bathymetry is progressive, as shape differences increase with time. The differences between the deposits generated by F2 and U2 currents are shown in Table 5. The average differences tend to grow with time, both the absolute and relative values. The maximum difference in deposit is one or two orders of magnitude greater the average. Its relative form is calculated based on the deposit of F2 existent on the location of the maximum difference. The results suggest that topography updates are as important in a flow that happens over the deposit of a previous current as in one that propagates over an initially flat surface. The relative errors calculated in F2 and U2 are a little higher than in F1 and U1, but remain at the same order of magnitude.

The deposits of U2 and F2 are settling over the deposits of previous simulations U1 and F1. Nevertheless, we wanted to compare the whole deposited material for each case, to see if there is any attenuation or reinforcement of the differences observed between F1 and U1 deposits. Comparisons of the whole deposit for each case, showing the amount deposited in each event are shown in Fig. 15. In some places, such as the region from $x = 0$ to $x = 2$, the errors are increased with

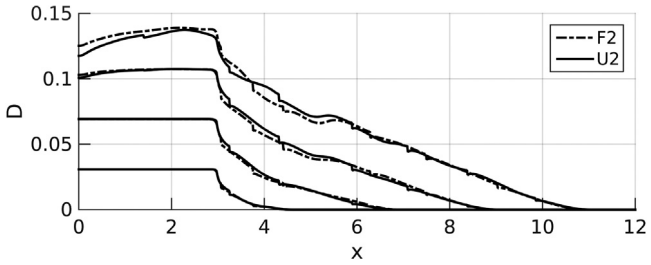

Fig. 14. Streamwise deposit averages on z direction, for cases F2 and U2, at $t = 5$, $t = 10$, $t = 15$ and $t = 20$ (curves from bottom to top).

Table 5
Differences in mass deposit between U2 and F2.

Time	Mean dif.	Relative mean dif.	Max. dif.	Relative max. dif.
$t = 5$	$4.3 \cdot 10^{-5}$	0.63%	$2.9 \cdot 10^{-3}$	14.92%
$t = 10$	$3.6 \cdot 10^{-4}$	1.97%	$5.1 \cdot 10^{-3}$	10.31%
$t = 15$	$1.1 \cdot 10^{-3}$	3.31%	$8.7 \cdot 10^{-3}$	26.55%
$t = 20$	$2.5 \cdot 10^{-3}$	4.70%	$1.1 \cdot 10^{-2}$	13.62%

the propagation of F2 and U2. The mean difference in deposit, after both events, is 0.036, representing 3.32% of the average value of total deposit. The relative error is very close to the one found for the first event, which is 3.58%. This evidence suggests that the relation between error and total deposit is maintained for the same channel configuration, even if there are events occurring one over another. Another possible analysis is that having an event propagating over another slightly attenuates the errors caused by the non-consideration of deposit feedback during the simulation. Although, further analysis should be conducted to corroborate these results.

6. Conclusion

We performed high-order Direct Numerical Simulations of tridisperse turbidity currents propagating over consolidated deposits. The

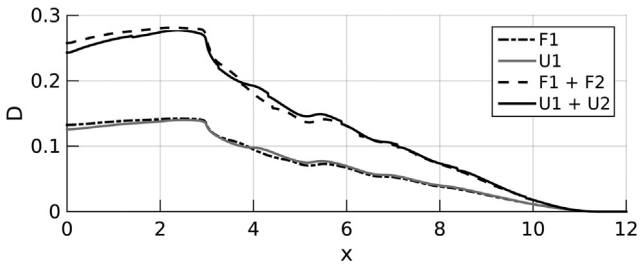

Fig. 15. Final deposits of simulations F1 plus F2, and U1 plus U2, averaged in z direction.

bathymetry was updated during the turbidity current event based on the deposited volume. The initial bathymetry was a horizontal bottom over which two currents propagated, one with topography update and another one maintaining the bottom flat. For these cases, the currents fronts evolution are the same, because both fronts propagated over the same flat terrain. On the other hand, for the parameters considered, the error in calculated deposit considering the deposit feedback can be larger than 10% in some regions of the domain, and its average value increases with time, attaining 3.58% at $t = 20$.

A second turbidity current was introduced over the bathymetry generated by deposits of the first current. Two cases were considered. One considers fixed topography and the other one updates the topography during the event. The difference on initial topography produces differences on the gravity current fronts. For both consecutive currents with fixed bottom, the deposit errors after $t = 20$ are similar.

With further research, it may be possible to understand more about the formation of submarine channels and fans using the model here presented. Granulometric curve, compactation factor and bathymetry data from natural currents can be employed as a base to simulate the propagation of turbidity currents and predict submarine landscape evolution.

Computer code availability

The open-source code used is Incompact3d, written in Fortran-90, and is available since 2006. Developers: Sylvain Laizet and Eric Lamballais. Sylvain Laizet contact address: Imperial College London, Department of Aeronautics, South Kensington Campus, London, SW7 2AZ, UK. Telephone number: +44 (0)20 7594 5045. E-mail: s.laizet@imperial.ac.uk. Fortran-90 and MPI compilers are required. The code was tested using Operating Systems Ubuntu 14.04, Ubuntu 16.04 and Ubuntu 18.04. Code and documentation can be found at www.incompact3d.com, on Downloads tab, or alternatively, on GitHub at github.com/xcompact3d, repository Old_Incompact3d Program size: 646 kB (source code), 4.6 MB (compiled). The code is licensed under GNU General Public License.

CRediT authorship contribution statement

Luísa Vieira Lucchese: conceptualization, formal analysis, investigation, methodology, validation, visualization, writing the original draft. **Leonardo Romero Monteiro:** methodology, formal analysis, writing - review & editing. **Edith Beatriz Camano Schettini:** project administration, supervision, formal analysis, writing - review & editing. **Jorge Hugo Silvestrini:** supervision, writing - review & editing.

Acknowledgments

This research was supported by Conselho Nacional de Desenvolvimento Científico e Tecnológico (CNPq). This research was developed with the support of *Núcleo Avançado de Computação de Alto Desempenho* (NACAD) from COPPE (Instituto Alberto Luiz Coimbra de Pós-Graduação e Pesquisa de Engenharia), Universidade Federal do Rio de Janeiro (UFRJ). This research was also supported by CENAPAD-SP (Centro Nacional de Processamento de Alto Desempenho em São Paulo), project UNICAMP/FINEP — MCTIC.

References

Bagnold, R.A., 1954. Experiments on a gravity-free dispersion of large solid spheres in a Newtonian fluid under shear. Proc. R. Soc. A 225 (1160), 49–63.
Benjamin, T.B., 1968. Gravity currents and related phenomena. J. Fluid Mech. 31 (02), 209–248.
Bouma, A.H., 1962. Sedimentology of Some Flysch Deposits: a Graphic Approach to Facies Interpretation. Elsevier Pub. Co..
Cantero, M.I., García, M.H., Balachandar, S., 2008. Effect of particle inertia on the dynamics of depositional particulate density currents. Comput. Geosci. 34 (10), 1307–1318.
Dairay, T., Lamballais, E., Laizet, S., Vassilicos, J.C., 2017. Numerical dissipation vs. subgrid-scale modelling for large eddy simulation. J. Comput. Phys. 337, 252–274.
Espath, L., Pinto, L., Laizet, S., Silvestrini, J., 2014. Two-and three-dimensional direct numerical simulation of particle-laden gravity currents. Comput. Geosci. 63, 9–16.
Espath, L., Pinto, L., Laizet, S., Silvestrini, J., 2015. High-fidelity simulations of the lobe-and-cleft structures and the deposition map in particle-driven gravity currents. Phys. Fluids (1994-present) 27 (5).
Francisco, E., Espath, L., Laizet, S., Silvestrini, J., 2018. Reynolds number and settling velocity influence for finite-release particle-laden gravity currents in a basin. Comput. Geosci. 110, 1–9.
Francisco, E.P., Espath, L., Silvestrini, J., 2017. Direct numerical simulation of bi-disperse particle-laden gravity currents in the channel configuration. Appl. Math. Model. 49, 739–752.
Gladstone, C., Phillips, J., Sparks, R., 1998. Experiments on bidisperse, constant-volume gravity currents: propagation and sediment deposition. Sedimentology 45 (5), 833–844.
Guerra, G.M., Zio, S., Camata, J.J., Rochinha, F.A., Elias, R.N., Paraizo, P.L., Coutinho, A.L., 2013. Numerical simulation of particle-laden flows by the residual-based variational multiscale method. Internat. J. Numer. Methods Fluids 73 (8), 729–749.
Harris, T.C., Hogg, A.J., Huppert, H.E., 2002. Polydisperse particle-driven gravity currents. J. Fluid Mech. 472, 333–371.
Härtel, C., Carlsson, F., Thunblom, M., 2000a. Analysis and direct numerical simulation of the flow at a gravity-current head. Part 2. the lobe-and-cleft instability. J. Fluid Mech. 418, 213–229.
Härtel, C., Meiburg, E., Necker, F., 2000b. Analysis and direct numerical simulation of the flow at a gravity-current head. Part 1. Flow topology and front speed for slip and no-slip boundaries. J. Fluid Mech. 418, 189–212.
Hoffmann, G., Nasr-Azadani, M.M., Meiburg, E., 2015. Sediment wave formation caused by erosional and depositional turbidity currents: A numerical investigation. Procedia IUTAM 15, 26–33.
Kovářík, K., Mužík, J., Masarovičová, S., Sitányiová, D., 2015. A local boundary integral method for two-dimensional particle-driven gravity currents simulation. Eng. Anal. Bound. Elem. 56, 119–128.
Kuenen, P.H., Migliorini, C., 1950. Turbidity currents as a cause of graded bedding. J. Geol. 91–127.
Kyrousi, F., Leonardi, A., Roman, F., Armenio, V., Zanello, F., Zordan, J., Juez, C., Falcomer, L., 2018. Large eddy simulations of sediment entrainment induced by a lock-exchange gravity current. Adv. Water Resour. 114, 102–118.
Laizet, S., Lamballais, E., 2009. High-order compact schemes for incompressible flows: A simple and efficient method with quasi-spectral accuracy. J. Comput. Phys. 228 (16), 5989–6015.
Laizet, S., Li, N., 2011. Incompact3d: A powerful tool to tackle turbulence problems with up to O (10^5) computational cores. Internat. J. Numer. Methods Fluids 67 (11), 1735–1757.
Lele, S.K., 1992. Compact finite difference schemes with spectral-like resolution. J. Comput. Phys. 103 (1), 16–42.
Lesieur, M., 2008. Turbulence in Fluids, Fluid Mechanics and its Applications. Springer, Dordrecht.
Lesieur, M., Métais, O., Comte, P., 2005. Large-Eddy Simulations of Turbulence. Cambridge University Press.
Lowe, D.R., 1982. Sediment gravity flows: Ii depositional models with special reference to the deposits of high-density turbidity currents. J. Sediment. Res. 52 (1).
Manica, R., 2009. Geração De Correntes De Turbidez De Alta Densidade: Condicionantes Hidráulicos E Deposicionais (Ph.D thesis). Universidade Federal do Rio Grande do Sul. Instituto de Pesquisas Hidráulicas. Programa de Pós-Graduação em Recursos Hídricos e Saneamento Ambiental.
Meiburg, E., Kneller, B., 2010. Turbidity currents and their deposits. Annu. Rev. Fluid Mech. 42, 135–156.
Nasr-Azadani, M., Hall, B., Meiburg, E., 2013. Polydisperse turbidity currents propagating over complex topography: comparison of experimental and depth-resolved simulation results. Comput. Geosci. 53, 141–153.
Nasr-Azadani, M., Meiburg, E., 2014. Turbidity currents interacting with three-dimensional seafloor topography. J. Fluid Mech. 745, 409–443.
Necker, F., Härtel, C., Kleiser, L., Meiburg, E., 2002. High-resolution simulations of particle-driven gravity currents. Int. J. Multiph. Flow. 28 (2), 279–300.
Paola, C., Voller, V.R., 2005. A generalized exner equation for sediment mass balance. J. Geophys. Res.: Earth Surf. 110 (F4).

Parsons, J.D., Friedrichs, C.T., Traykovski, P.A., Mohrig, D., Imran, J., Syvitski, J.P., Parker, G., Puig, P., Buttles, J.L., Garcia, M.H., 2007. The mechanics of marine sediment gravity flows. In: Nittrouer, C., Austin, J., Field, M., Syvitski, J., Wiberg, P. (Eds.), Continental Margin Sedimentation: From Sediment Transport to Sequence Stratigraphy. Blackwell, Oxford, UK, pp. 275–333.

Peskin, C.S., 2002. The immersed boundary method. Acta Numer. 11, 479–517.

Rubey, W.W., 1933. Settling velocity of gravel, sand, and silt particles. Amer. J. Sci. (148), 325–338.

Shanmugam, G., 2000. 50 years of the turbidite paradigm (1950s—1990s): deep-water processes and facies models—a critical perspective. Mar. Pet. Geol. 17 (2), 285–342.

Simpson, J.E., 1999. Gravity currents in the environment. Proc. Indian Nat. Sci. Acad. A 65, 1–26.

Stow, D.A., Shanmugam, G., 1980. Sequence of structures in fine-grained turbidites: comparison of recent deep-sea and ancient flysch sediments. Sediment. Geol. 25 (1–2), 23–42.